Smart Monitoring of Corrosion Damage of Shield Tunnel Lining Segment through PZT-based Active Sensing Aided with a Fused Deep Learning Network

Chuan Zhang
Key Laboratory of Transportation Tunnel Engineering, Ministry of Education, Southwest Jiaotong University, Chengdu 610031, China; e-mail: zhangchuan@my.swjtu.edu.cn

Yifeng Zhang

Zachry Department of Civil & Environmental Engineering, Texas A&M University, TX 77843, USA; e-mail: tamu.zyf@gmail.com

Zhengyu Xiong
Key Laboratory of Transportation Tunnel Engineering, Ministry of Education, Southwest Jiaotong University, Chengdu 610031, China; e-mail: xzy@my.swjtu.edu.cn

Zhengshu He**(Corresponding author)*
Key Laboratory of Transportation Tunnel Engineering, Ministry of Education, Southwest Jiaotong University, Chengdu 610031, China; e-mail: zhengshuhe91@swjtu.edu.cn

Qixiang Yan

Key Laboratory of Transportation Tunnel Engineering, Ministry of Education, Southwest Jiaotong University, Chengdu 610031, China; e-mail: yanqixiang@home.swjtu.edu.cn

ABSTRACT

Shield tunnel segmental linings are critical components of underground transportation infrastructures, providing stability and support to tunnel structures. However, they are vulnerable to corrosion damage due to exposure to harsh environmental conditions during the long-term service period. Corrosion damage in shield tunnel linings can lead to various structural issues, including reduced load-bearing capacity, increased vulnerability to collapse, and compromised safety for both structures and passengers. By implementing structure health monitoring (SHM), engineers can ensure the safety, durability, and economic viability of shield tunnels. Real-time monitoring allows for timely interventions, while the insights gained from SHM data enable the development of effective corrosion prevention strategies. Ultimately, SHM enhances the overall performance and longevity of shield tunnel infrastructure, contributing to the sustainable development of transportation and utility systems. As a promising nondestructive testing (NDT) technique, the PZT-based active sensing method has been extensively applied to many aspects in structure health monitoring. In this paper, this method was employed to monitor the corrosion damage of reinforced concrete (RC) tunnel lining segments. Due to the fact that in practical situations, tunnel lining segments are both subjected to corrosion and external loads simultaneously, the coupling of loading and corrosion effects result in more severe damage and deterioration of segments. Therefore, accelerating corrosion tests of bended RC lining segments were performed. Firstly, the damage behaviors of RC segments were investigated according to corrosion and loading tests. Subsequently, the variation of collected stress wave signals of PZT sensors was interpreted primarily based on the wavelet packet analysis. The highlight of this study is that a two-dimensional convolutional neural network-based (CNN) deep learning (DL) hybrid network was constructed and well trained to identify different damage phases from image-based datasets of continuous wavelet packet (CWT) spectra. The results well demonstrate the effectiveness and high accuracy of the DL model, which facilitates smart monitoring and automatic classification of corrosion damage of RC tunnel linings without manual feature extraction.

KEYWORDS: piezoelectric materials, active sensing, deep learning, corrosion damage, tunnel lining.

1. INTRODUCTION

Monitoring of the corrosion damage of reinforced concrete (RC) shield tunnel linings plays a pivotal role in ensuring the structural integrity and operational safety of underground transportation systems, given that a huge amount of shield tunnels have been extensively constructed in many coastal cities in China (He, He, Kang, Huang, Wang and Xu, 2023, He, He, Ma, Yang and Kang, 2023). Shield tunnels serve as lifelines for urban infrastructure, facilitating the smooth operation of subways, metro networks, and utility conduits. However, these critical infrastructures are easily susceptible to the corrosion-induced deterioration in marine corrosive environments, which can compromise their long-term performance and stability. Moisture, excessive loads, chemical agents, coupled with various environmental factors, can accelerate the corrosion process, leading to material degradation and potential structural failures (He, He, Ma, Yang and Xu, 2023). Therefore, effective monitoring of corrosion in shield tunnel segmental linings is crucial for early detection, timely intervention, and appropriate maintenance.

Up to now, numbers of advanced approaches have demonstrated the effectiveness and reliability in detecting the corrosion damage of RC structures, mainly including the acoustic emission (AE) (He, He, Ma, Wang and Huang, 2022, Patil, Karkare and Goyal, 2017, Verstrynge, Steen, Vandecruys and Wevers, 2022), digital image correlation (DIC) (Wang, Jin, Liu, Chen, Feng and Tang, 2021), X-ray computed tomography (CT) (Steen, Pahlavan, Wevers and Verstrynge, 2019), etc. Despite that these methods could provide accurate measurements, most of them necessitate bulky and costly data acquisition devices, greatly limiting their practical applications. Thus, it is in great demand to develop more applicable sensing techniques. In recent years, there has been significant progress in various nondestructive testing (NDT) methods applied in the realm of structural health monitoring (SHM). One prominent technique is known as the wave propagation-based method, utilizing piezoelectric lead zirconate titanate (PZT) smart materials with robust piezoelectric properties. This method leverages both the direct and inverse piezoelectric effects and employs at least a pair of PZT transducers to actuate and receive stress wave signals through to-be-tested structures. As the excited waves travel through the transmission medium, any property changes or damages within the medium will influence the wave propagation and energy attenuation characteristics. By using mainstream signal processing methods such as the wavelet packet transform and the windowed Fourier transform, the accurate damage detection and evaluation of tested structures could be realized. This serves as the fundamental principle of the wave propagation method in SHM. Due to its real-time, remote, and autonomous monitoring capabilities, along with its cost-effectiveness, this method has broadly been applied to many SHM aspects. More impressively, through the coordination of latest artificial neural networks in processing stress wave signals, it has great potentials to be evolved into a more intelligent sensing technique, which enables automatic signal identification and accurate damage assessment (Kong, Ji, Gu, Chen and Yuan, 2022, Yan, Liao, Zhang, Zhang, Luo and Zhang, 2022). So far, very rare literature could be found regarding the monitoring and assessment of the corrosion damage of RC tunnel linings through the integration of the wave propagation method with DL networks.

The aim of this study is to demonstrate the applicability of the DL-aided wave propagation method for monitoring and assessing corrosion damage in reinforced concrete (RC) tunnel linings. To achieve this, we conducted a series of experiments, including an accelerated corrosion test on a prototype RC segment subjected to sustained loads. We thoroughly investigated the deformation characteristics and corrosion-induced cracking behaviors of the bended RC segment. Additionally, we analyzed the time-domain stress wave signals and continuous wavelet transform (CWT) spectra throughout the accelerated corrosion process. Notably, our research introduced a hybrid DL framework designed to automatically identify CWT spectra, enabling accurate classification of corrosion damage without the need for manual feature extraction.

2. EXPERIMENTAL INVESTIGATION

2.1. *Specimen preparation*

The accelerated corrosion test and SHM measurements were performed on a fabricated prototype RC segment with the width, thickness and curved length of 1500.0 mm, 350.0 mm and 3533.3 mm, respectively. The detailed geometric parameters and layouts of steel reinforcements are exhibited in **Figure 1**. In addition, ordinary Portland cement, fine sands, gravels with a maximum aggregate size of 30.0 mm were evenly blended with pure water and water reducer to cast the concrete. The water to cement ratio is controlled at 0.40, and the specific proportions of concrete mixtures are listed in **Table 1**. The compressive and tensile strengths of concrete are 41.6 MPa and 2.85 MPa, respectively. Moreover, different steel grades were selected for longitudinal steel bars and stirrup, the main mechanical properties are given in **Table 2**.

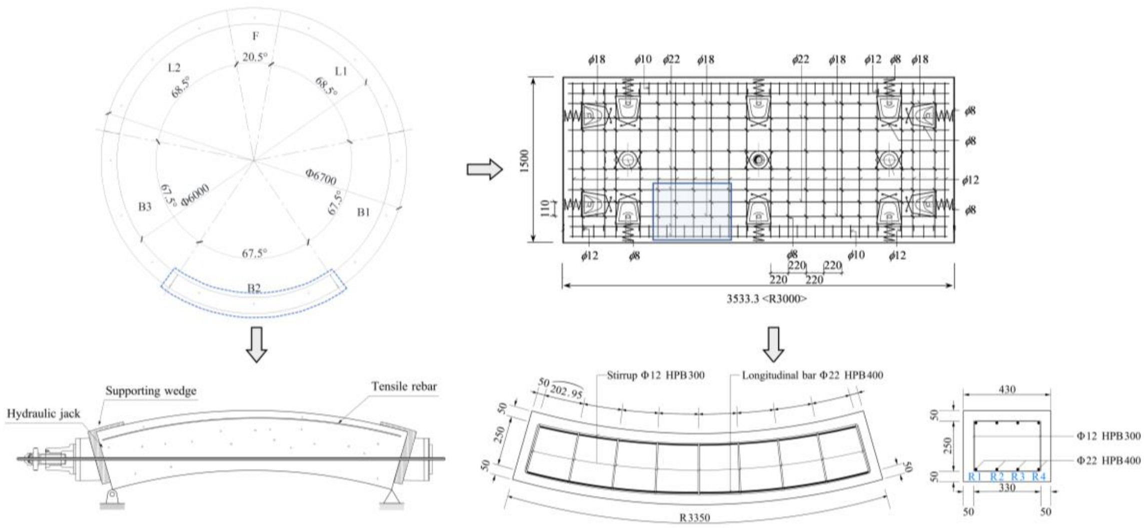

Figure 1 Design of the bended RC tunnel lining segment.

Table 1 Concrete mix proportion(kg/m^3).

w/c ratio	cement	fine sand	gravel	water reducer	water
0.40	325	677	1167	6.3	130

Table 2 Material properties of reinforcements.

category	type	diameter (mm)	yield strength (MPa)	tensile strength (MPa)
longitudinal	HRB400	22	400	540
stirrup	HPB300	12	300	420

2.2. *Experiment setup and procedures*

The entire experimental setup is displayed in **Figure 2**. As is shown, before the initiation of the accelerated corrosion of the RC segment, a constant load of 465.0 kN was first applied to both ends of the segmental specimen, so as to simulate the practical conditions of axial force and bending moment. Later, the electrochemical accelerated corrosion was performed on the RC segment via a current-through plastic container filled with 3% sodium chloride (NaCl) solution. The rectangular container with a dimension of 800×1500×10 mm was located at the center area of the top surface of the segment. In addition, a stainless-steel mesh immersed in the electrolyte served as the cathode, meanwhile two tensile steel rebars embedded in test segmental specimen were chosen as the anode. To assure the target corrosive damage of the longitudinal rebars in tension zone within a designed period, a constant current of 1.10 A was continuously passed through the tensile rebars in the tested segment. In this experiment, the corrosion test lasted 30 days, and the targeted corrosion damage degree was roughly set to 10%, which could be characterized by the average loss of the diameter of the tensile rebars based on the Faraday's second law. Moreover, a displacement gauge was placed at the mid-span bottom of the specimen to acquire the load-deformation curve.

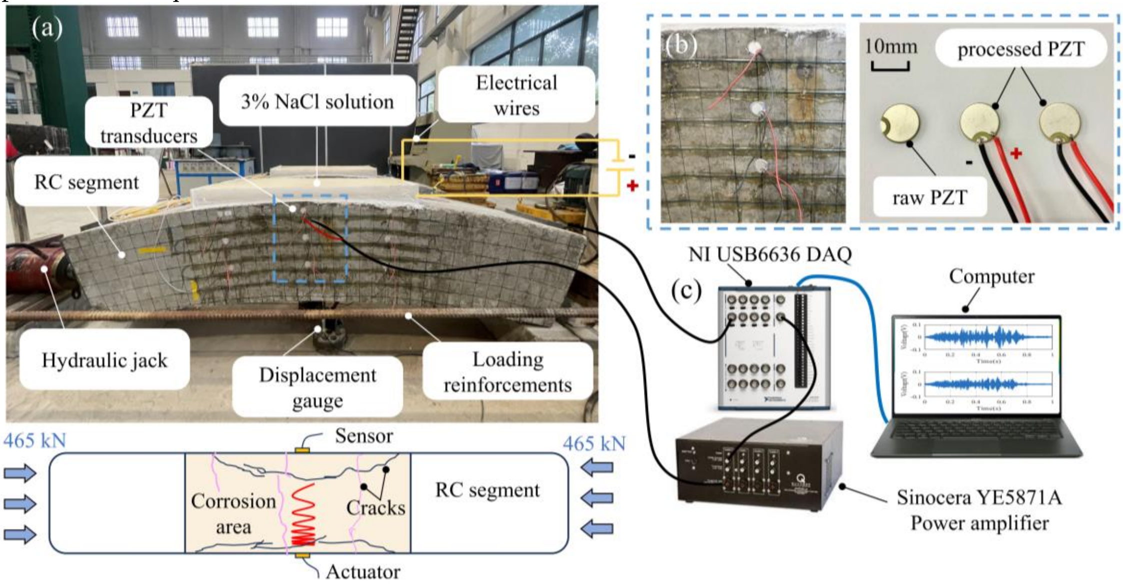

Figure 2 Experimental setup.

For the implementation of the wave propagation-base method, a pair of circular-shaped processed PZT patches with a diameter of 10.0 mm and a thickness of 1.0 mm (covered with a thin coating of electricity-resistant and waterproof liquid tapes) were epoxy-pasted along the center lines within both the side surfaces, 20.0 mm away from the upper surface of the segment. The wave propagation measurement was conducted simultaneously with the corrosion test. During the measurement, the PZT actuator was excited by an input electric signal to emit a sweep sine wave signal, the frequency of which increases linearly from 1.0 to 500.0 kHz in a duration of 1.0 s and the amplitude is 10.0 V. Furthermore, the excited signal was amplified threefold by a power amplifier. In each test, the sampling rate is controlled at 1.0 MHz and the data was repetitively recorded five times. A total of 10 measurements were performed throughout the corrosion process.

3. NEURAL NETWORK ARCHITECTURE

In this paper, a 2D CNN-BiLSTM hybrid model was developed to detect corrosion damage of prototype segment via wave propagation technique, continuous wavelet transform (CWT) and DL algorithms.

For the purpose of establishing the dataset, the following signal preprocessing work was carried out. The initial signals were captured through wave propagation technique and further augmented by adding Gaussian noise with five SNRs. Subsequently, a common signal time-frequency conversion method, CWT, was introduced to convert the augmented signals into time-frequency spectra, which makes its calculation according to the Eq. (1) below (Zhang, Yan, Zhang, Liao and Zhong, 2023):

$$W(u,\tau) = \frac{1}{\sqrt{u}}\int_{-\infty}^{\infty} x(t)\psi^*\left(\frac{t-u}{\tau}\right)dx \tag{1}$$

where $x(t)$ is the original signal, u denotes scale parameter, τ refers to position parameter and $\psi^*(x)$ signifies complex conjugate of wavelet function $\psi(x)$ And Morl was chosen to serve as the wavelet for CWT. To increase the computational efficiency, the spectra were grayed out and saved as a dataset for model training.

In terms of the 2D CNN-BiLSTM hybrid model, it was designed as the fusion of CNN module, BiLSTM module and output layer successively. This model inherited the strengths of both CNN and BiLSTM. As the very beginning of the 2D CNN-BiLSTM hybrid model, CNN was originally applied as a powerful image recognition network, and the formulas of the convolution calculation could be expressed as Eq. (2) and (3) (Liao, Yan, Zhong, Zhang and Zhang, 2023):

$$x_k^l = \sum_{i=1}^{N} \mathrm{conv2D}(\mathrm{w}_{ik}^{l-1}, \mathrm{s}_i^{l-1}) + b_k^l \tag{2}$$

$$y_k^l = f(x_k^l) \tag{3}$$

where x_k^l represents the output before activation, w_{ik}^{l-1} is the filter, s_i^{l-1} refers to the output of previous layer, b_k^l signifies the bias, $conv2D(.)$ denotes 2D convolution, y_k^l is the output after activation, $f(x)$ is defined as activation function. The addition of CNN module could provide great machine visualization for the network. Thus, a total of four convolutional layers, two max-pooling layers and one flatten layer are set into the network as CNN modules. BiLSTM, on the other hand, could provide the network with the ability to efficiently process excess data as well as address gradient vanishing. The internal workflow of BiLSTM is expressed as the following Eq. (4), (5) and (6):

$$\vec{h}_t = f_f(x_t, \vec{h}_{t-1}) \tag{4}$$

$$\overleftarrow{h}_t = f_b(x_t, \overleftarrow{h}_{t+1}) \tag{5}$$

$$y_t = W_y[\vec{h}_t, \overleftarrow{h}] + b_y \tag{6}$$

where $\vec{h}_t$ and $\overleftarrow{h}_t$ represent the outputs of the forward and backward hidden layers, respectively. x_t denotes the input vector. $f_f(\cdot)$ and $f_b(\cdot)$ signify the activation functions in the forward and backward directions, respectively. W_y and b_y are the weight and bias matrices, respectively. $[,]$ denotes the concatenation of vectors. With the help of BiLSTM module, the network can make fuller use of the information from the input data. Hence, 128 BiLSTM cells were added as BiLSTM modules in 2D CNN-BiLSTM hybrid model. At the end of the hybrid model, output layer was arranged as a fully connected (FC) layer and a Softmax function, which was utilized to output the classification of the corrosion damage. The 2D CNN-BiLSTM hybrid model was implemented in Python 3.6 language environment with Tensorflow library and Keras API. The detailed flowchart and parameters are illustrated in **Figure 3** and **Table 3**, respectively.

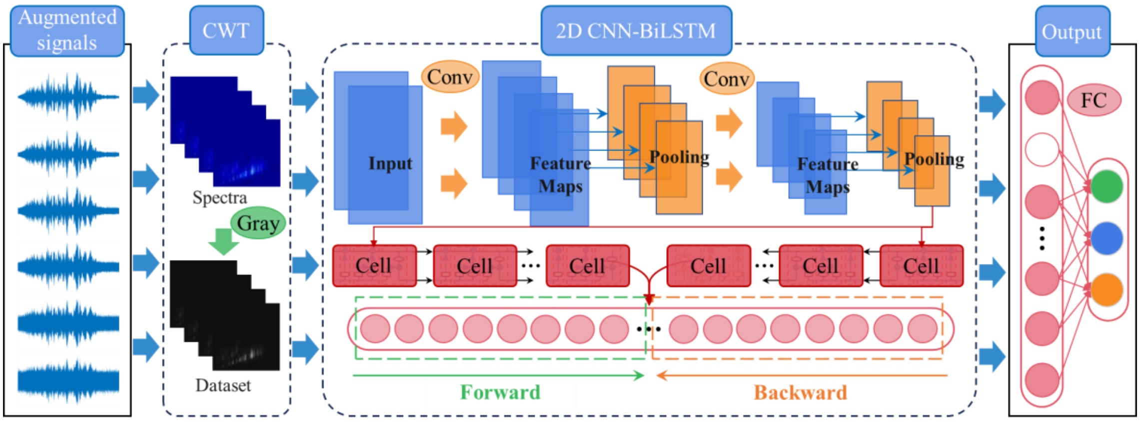

Figure 3 Flowchart of the 2D CNN-BiLSTM hybrid model in corrosion damage detection.

Table 3 Detailed parameters of the 2D CNN-BiLSTM hybrid model.

Layer	Type	Parameter settings
L1	Conv2D	Filters=32, kernel size=3×3, strides=2×2, padding="same", activation="ReLU"
L2	Conv2D	Filters=32, kernel size=3×3, strides=2×2, padding="same", activation="ReLU"
L3	Max-pooling	Kernel size=2×2, strides=1×1, padding="valid"
L4	Conv2D	Filters=64, kernel size=3×3, strides=1×1, padding="same", activation="ReLU"
L5	Conv2D	Filters=64, kernel size=3×3, strides=1×1, padding="same", activation="ReLU"
L6	Max-pooling	Kernel size=2×2, strides=1×1, padding="valid"
L7	Flatten	Feature serialization
L8	BiLSTM	Cells=128, merge mode="concat"
L9	FC	Units=500, dropout rate=0.1, activation = "ReLU"
L10	FC	Units=300, dropout rate=0.1, activation = "ReLU"
L11	FC	Units=3, activation="Softmax"

4. NEURAL NETWORK ARCHITECTURE

4.1. *Corrosion damage evolution*

The mid-span deformation of the corroded RC segment is presented in **Figure 4**. As is shown, three stages could be evidently observed, including the acceleration stage, stable stage, and uplift stage. Soon after the initiation of the corrosion process, the deformation presents a significantly increasing trend, later followed by a roughly constant tendency from 9 to 21 d. Subsequently, the curve continues to go upwards with the proceeding corrosion of the steel reinforcements. It is known that the cracks along the longitudinal direction are viewed as the results from the corrosive swelling within the RC specimen. Thus, to better characterize the corrosion damage of the RC segment, the progression of longitudinal cracks within both side surfaces was explored, the results are also exhibited in **Figure 4**. The curve of the corrosion crack length also shows three stages, well conforming to the mid-span deformation curve.

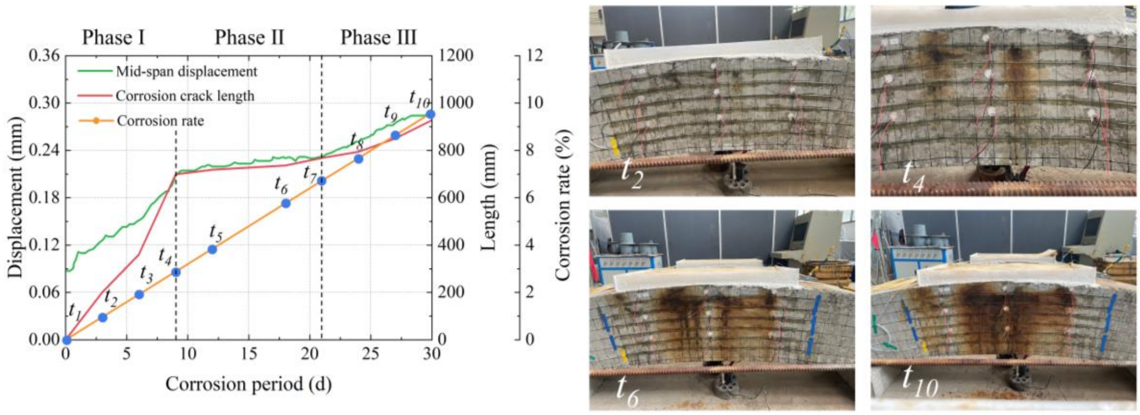

Figure 4 Progressive corrosion damage of the bended RC tunnel segment.

4.2. *Signal variation*

The variations of raw time-domain signals and CWT time-frequency spectra throughout the corrosion test are given in **Figure 5**, in which a total number of 10 signals corresponding to specified moments are displayed. As is displayed, there are multiple clusters in the original stress wave signals. As the corrosion proceeded from t1-t3, the amplitude and energy of the signals declined greatly, suggesting the accelerating corrosion damage. Afterwards, the wave signal remains approximately unchanged, which is in good accordance with the stable corrosion stage. This is mainly attributed to the phenomenon that the constantly generated corrosion products fill in the cracks and prevent them from expansion. Later, as more and more corrosion products accumulate, the cracks further grow and propagate due to the swelling effect, which greatly impedes the wave propagation through the corroded RC segment. This is also reflected from the received stress wave signals, which have very low amplitude and energy.

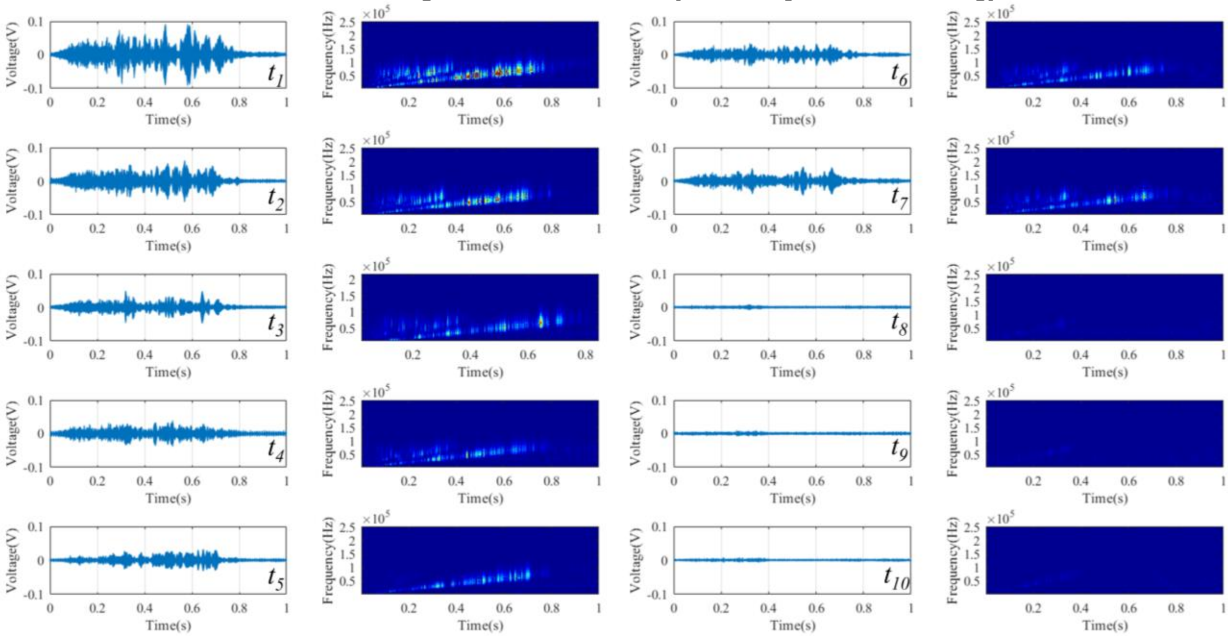

Figure 5 Variation of stress wave signals and CWT spectra.

4.3. *Model training*

To better train the model, the original data was augmented and Gaussian noise with SNRs of 0, 5, 10, 15, and 20 were respectively added to each original stress wave signal. As a result, a total of 50 × 6 = 300 sets of signals were obtained. Next, the augmented signals were converted into time-frequency spectra with single color channel and saved as a dataset. Moreover, the samples in the dataset were disrupted and randomly separated into a training set and a testing set, following the ratio of 2:1. And the normalization was carried out on every data in the dataset to improve the convergence of the training process.

Subsequently, the training process, containing 30 epochs, was conducted on a computer with a CPU of i5-12400F, 2.50GHz, a GPU of GTX 1650S and 16g RAM. The accuracy and loss curves of the training process are shown as **Figure 6**. Overall, the training process did not show noticeable overfitting, only exhibiting slight overfitting at the 8th and 13th epochs. The loss of training set and validation set basically stopped declining after 18 epochs of training, while both of the accuracy curves exceeded 96.30%. And up to the end of model training, the accuracy of training set and validation set remained essentially stabilized and finally climbed to 100% and 99.93%, respectively. It could be obviously indicated that the model was well-trained with high accuracy and good convergence.

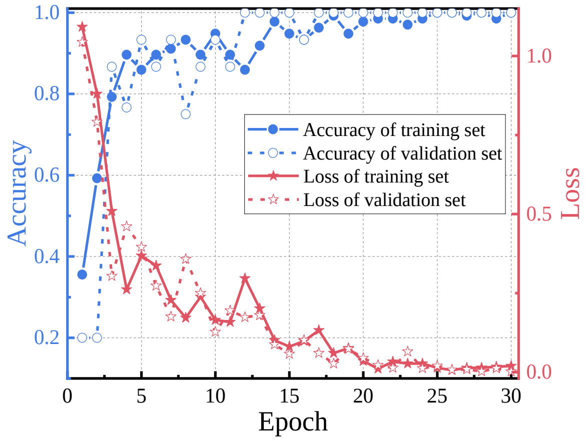

Figure 6 Accuracy and loss curves for training and validation sets.

4.4. *Classification of concrete fiber content*

The testing results of the model are presented in the form of a confusion matrix, as shown in **Figure 7**. Larger values on the diagonal in the confusion matrix indicate higher classification accuracy. It was obvious that each case had an extraordinary accuracy with case 2 and case 3 even achieving 100%. On the whole, the testing process was performed with a considerable accuracy, 99.00%. In order to visualize the testing result more intuitively, the t-distributed Stochastic Neighbor Embedding (t-SNE) technique was applied to show the testing result of the model. Each data in the input layer as well as the FC layer was visualized by spotting in the figure, as shown in **Figure 8**. The result indicated that the signals under different cases were clearly distinguished from the initial chaotic distribution. All of the above demonstrated that the model had a excellent ability to classify concrete corrosion damage based on stress wave signals.

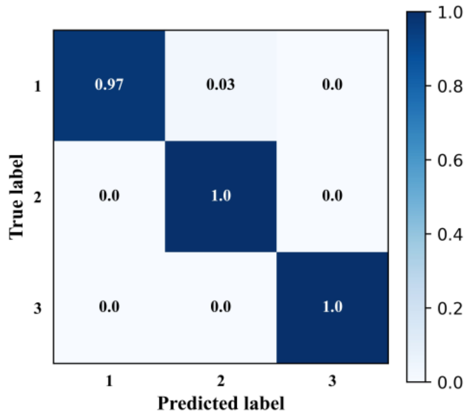

Figure 7 Confusion matrices of classification results of corrosion damage.

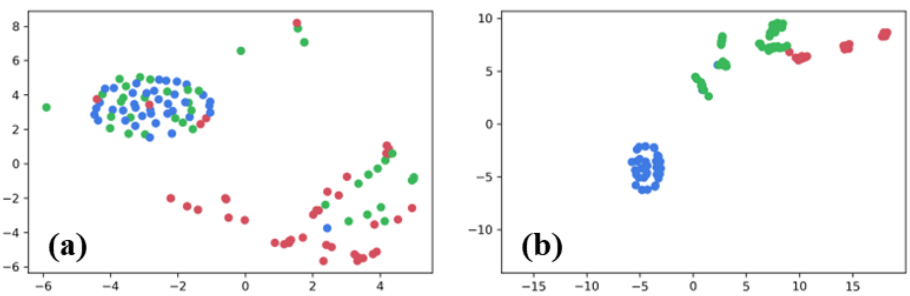

Figure 8 Visualization of feature vectors via the t-SNE: (a) denotes the input layer; (b) denotes the FC layer.

To exhibit the superiority of the model introduced in this paper, the comparison analysis of the 2D CNN-BiLSTM hybrid model with common ML models and DL models was carried out. ML models included decision tree (DT), support vector machine (SVM) and back propagation neural network (BPNN) and the power spectrum densities (PSD) calculated at ten frequency ranges from original signals were selected as their features. The specific frequency ranges and the parameters of the ML models are shown in **Table 4** and **Table 5**. DL models included 2D CNN and BiLSTM, and their parameters were just set as the CNN module and BiLSTM module from 2D CNN-BiLSTM hybrid model. Through comparative analysis, it could be observed that the classification accuracy of DL models was higher than that of ML as a whole. The best-performing ML model, BPNN, still only achieved accuracy of 83.98%, while the best-performing DL model, 2D CNN-BiLSTM hybrid model, could reach up to 99.00%, approximately 5% higher than that of 2D CNN and BiLSTM. Consequently, it could be concluded that the classification performance of 2D CNN-BiLSTM hybrid model is better than the ML models, 2D CNN and BiLSTM.

Table 4 Features extracted based on PSD

Feature name	1	2	3	4	5	6	7	8	9	10
Frequency band (kHz)	0-30	30-60	60-90	90-120	120-150	150-180	180-210	210-240	240-270	270-300

Table 5 Parameter settings of comparative ML models

Methods	Parameter settings
DT	Depth of tree=100, minimum sample split=2, minimum sample leaf=1
SVM	Kernel function=radial basis function, kernel width=5.5, regularization parameter=0.05
BPNN	Input layer: neuron number=10, activation= “ReLU”. hidden layer: neuron number=128, activation= “ReLU”. output layer: neuron number=6, activation= “Softmax”. optimizer= “SGD”

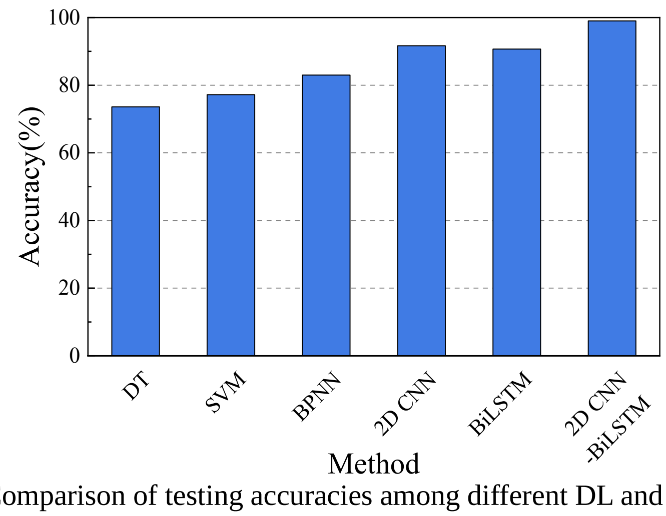

Figure 9 Comparison of testing accuracies among different DL and ML models.

5. CONCLUSIONS

This paper set out to demonstrate the practicality of the DL-aided wave propagation method for monitoring and evaluating corrosion damage in RC tunnel linings. To accomplish this, accelerated corrosion experiments were carried out on a prototype segment. Simultaneously, PZT-based wave propagation technique was utilized to the experiment to capture the signal response of the segment at different levels of corrosion. By analyzing the crack extension of the segment at different periods of corrosion, the corrosion process of the prototype segment was divided into three stages, which corresponded well with the captured signals and their time-frequency spectra. On this basis, this paper also innovatively introduced a 2D CNN-BiLSTM hybrid model which could realize to classify the signals under different corrosion stages with excellent accuracy of 99% and great convergence. The superiority of the 2D CNN-BiLSTM hybrid model was further illustrated by comparing the training results with other common ML models (DT, SVM, BPNN) and DL models (2D CNN, BiLSTM). In conclusion, the proposed model exhibits a strong capability in classifying the corrosion level of the prototype tunnel lining.

CONFLICT OF INTERESTS

The authors declare that they have no known competing financial interests or personal relationships that could have appeared to influence the work reported in this paper.

ACKNOWLEDGEMENTS

The authors gratefully acknowledge financial supports for this research provided by the National Natural Science Foundation of China (Grant Number: 52208407, 52278416, U21A20152) and the fellowship of China Postdoctoral Science Foundation (2022 M712640).

REFERENCES

He, Z., He, C., Kang, X., Huang, X., Wang, S. and Xu, G. 2023. Effects of sustained load and reinforcement spacing on the evolution and spatial characteristics of corrosion damages in RC segmental specimens, *Construction and Building Materials*, 407.

He, Z., He, C., Ma, G., Yang, W. and Kang, X. 2023 Performance assessment of partially corrosion-damaged RC segment incorporating the spatial variability of steel corrosion, *Construction and Building Materials*, 371.

He, Z., He, C., Ma, G., Yang, W. and Xu, G. 2023. Performance assessment of deteriorated RC shield tunnels integrated with stochastic field-based modeling for nonuniform steel corrosion, *Engineering Failure Analysis*, 148.

He, Z., He, C., Ma, G., Wang, S. and Huang, X. 2022. Experimental investigation on the deterioration process and spatial variation of corrosion damage of RC segmental specimens under sustained load, *Construction and Building Materials*, 349.

Verstrynge, E., Van Steen, C., Vandecruys, E. and Wevers, M. 2022. Steel corrosion damage monitoring in reinforced concrete structures with the acoustic emission technique: A review, *Construction and Building Materials*, 349.

Wang, X., Jin, Z., Liu, J., Chen, F., Feng, P. and Tang, J. 2021. Research on internal monitoring of reinforced concrete under accelerated corrosion, using XCT and DIC technology, *Construction and Building Materials*, 266.

Van Steen, C., Pahlavan, L., Wevers, M. and Verstrynge, Els. 2019. Localisation and characterisation of corrosion damage in reinforced concrete by means of acoustic emission and X-ray computed tomography, *Construction and Building Materials*, 197: 21-29.

Kong, Q., Ji, K., Gu, J., Chen, L. and Yuan, C. 2023. A CNN-integrated percussion method for detection of FRP–concrete interfacial damage with FEM reconstruction, *Structural Health Monitoring*, 22(1): 216-231.

Yan, Q., Liao, X., Zhang, C., Zhang, Y., Luo, S., and Zhang, D. 2022. Intelligent monitoring and assessment on early-age hydration and setting of cement mortar through an EMI-integrated neural network, *Measurement*, 203.

Zhang, C., Yan, Q., Zhang, Y., Liao, X. and Zhong, H. 2023. Intelligent monitoring of concrete-rock interface debonding via ultrasonic measurement integrated with convolutional neural network, *Construction and Building Materials*, 400.

Liao, X., Yan, Q., Zhong, H., Zhang, Y., and Zhang, Chuan. 2023. Integrating PZT-enabled active sensing with deep learning techniques for automatic monitoring and assessment of early-age concrete strength, *Measurement*, 211.